Beam Collimation System for a 16 GeV Proton Driver [1]

A. I. Drozhdin[2], C. J. Johnstone and N. V. Mokhov
Fermi National Accelerator Laboratory
P.O. Box 500, Batavia, Illinois 60510

Abstract

It is shown that with the appropriate lattice and collimation design, one can control beam loss in the 16 GeV Fermilab Proton Driver. Based on detailed Monte-Carlo simulations, a *3-stage collimation system* is proposed which consists of primary, secondary and supplementary collimators located in a special 60 m long injection section along with a painting system. It allows localization of more than 99% of beam loss to this section with only a 0.3 W/m (on average) beam loss rate in the rest of the machine. As a result, beam loss and induced radiation effects in lattice elements can be reduced to levels which are defined as acceptable.

1 INTRODUCTION

The proton driver under design at Fermilab is a 16 GeV high intensity rapid cycling proton synchrotron [1, 2]. A very high beam power—1.2 MW in phase-I and 4 MW in phase-II—implies serious constraints on beam losses in the machine. The main concern are the hands-on maintenance and ground-water activation [3]. Only with a very efficient beam collimation system can one reduce uncontrolled beam losses to such an extent that the machine can meet the criteria established for allowable radiation levels.

Table 1: Proton Driver phase-I parameters.

Injection kinetic energy (GeV)	0.4
Top kinetic energy (GeV)	16
Circumference (m)	632.114
Painting injection duration (μs)	90
Dipole field (T)	1.354
Injected 95% emittance ε_N (mm.mrad)	2.6
After painting emittance ε_N (mm.mrad)	50
Protons per bunch at extraction	7.5×10^{12}
Number of bunches	4
Total intensity at extraction	3×10^{13}
Repetition rate (Hz)	15
Longitudinal emittance (eV$\times$s)	0.1
RF frequency (MHz)	53

The parameters of the preliminary 16 GeV Proton Driver racetrack lattice used in this study are presented in Table 1. There are two long straight sections in the ring. The first one, 90 m long with zero dispersion, is used for RF system and extraction. The second one (60 m long) is used for injection and beam halo collimation. The β-functions and dispersion in the entire ring are shown in Fig. 1.

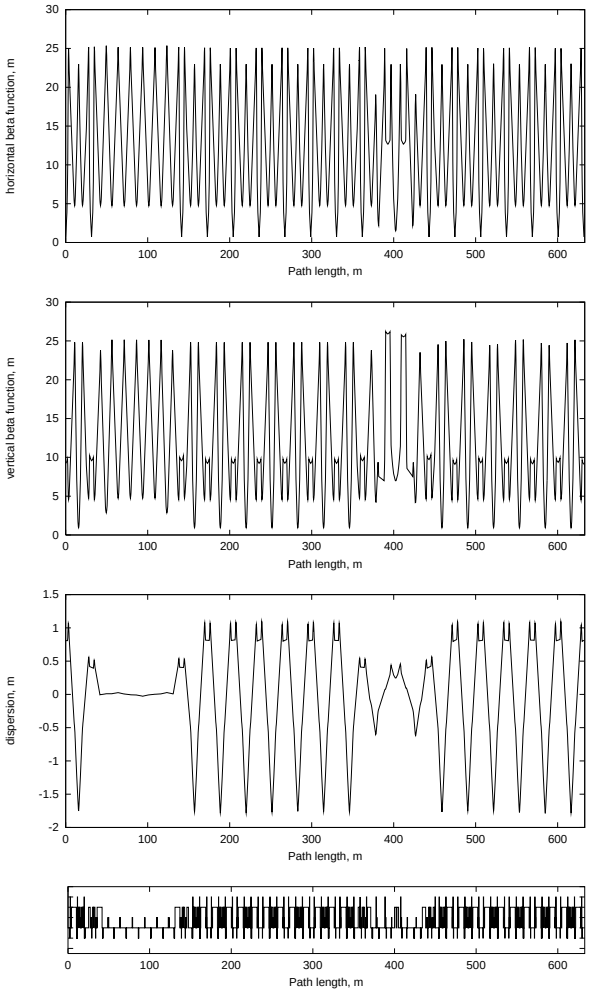

Figure 1: Lattice β-functions and dispersion.

A multi-turn particle tracking is performed through the accelerator which includes beam halo interactions in the collimators using the STRUCT [4] code. Realistic strengths along with aperture restrictions are taken into account for individual lattice components during these calculations. Particles lost in the accelerator are stored into input files for the next step in the study. With these input files, full-scale Monte-Carlo hadronic and electromagnetic shower simulations are done for the lattice and tunnel components, including shielding with realistic geometry, materials and magnetic field, using the MARS [5] code. For such calculations, it is assumed that 10% of the beam is lost at injection and 1% is lost at the ramp and flat top.

The injection section β-functions, beam size after painting, and dispersion are shown in Fig. 2. The separation needed between the circulating proton beam and the injected H^- beam is provided by two 2 m long accelerator magnets located on both sides of the foil (Fig. 3). At the quadrupole doublet the separation is 389 mm, allow-

[1]Work supported by the U. S. Department of Energy under contract No. DE-AC02-76CH03000
[2]e–mail: drozhdin@fnal.gov

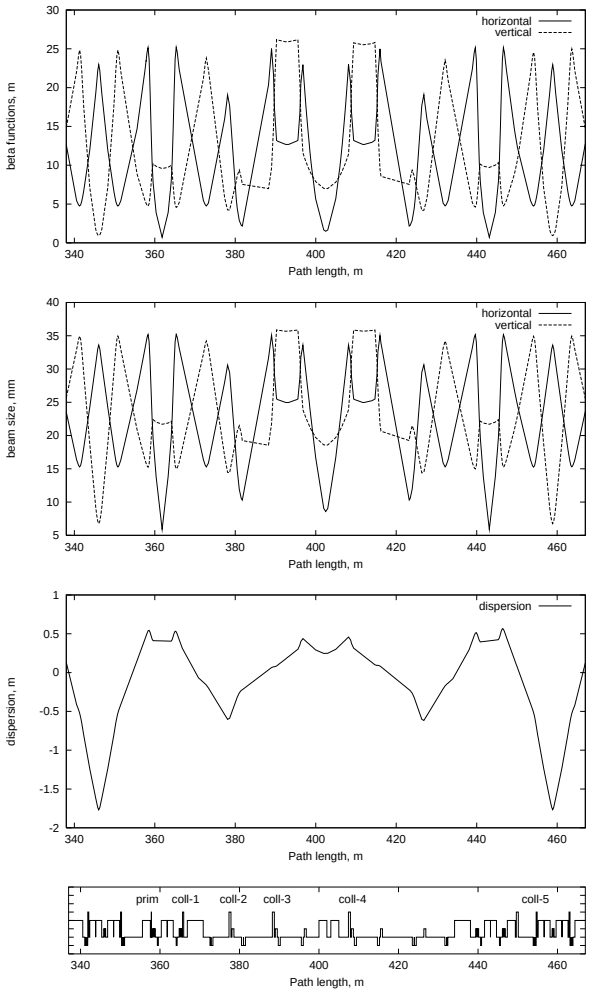

Figure 2: Injection section β-functions, beam size after painting and dispersion.

ing the H^- beam to bypass the quadrupole. Injection painting is used to provide a uniform density distribution of the beam in the transverse plane and is accomplished using two 0.5 m long fast-ramping orbit bump magnets. These magnets move the circulating proton orbit at the beginning of injection by 10.25 mm onto a thin graphite stripping foil located in the middle of the straight section. The overlay of the proton orbit relative to the H^- trajectory and, hence, the density distribution, is controlled using the detailed ramp of these orbit bump magnets whose maximum field reaches 3 kG. A collimator between the doublet and the stripping foil is used to absorb residual neutral components.

2 COLLIMATION AT TOP ENERGY

The beam power at the top energy in phase-I is 1.2 MW. At 16 GeV in the arc of the considered lattice, the limits for hands-on maintenance are 0.25 W/m in the bare beam pipes and 3 W/m in magnets, while the ground-water limit is 0.6 W/m [3]. Calculations performed for a slow rate of

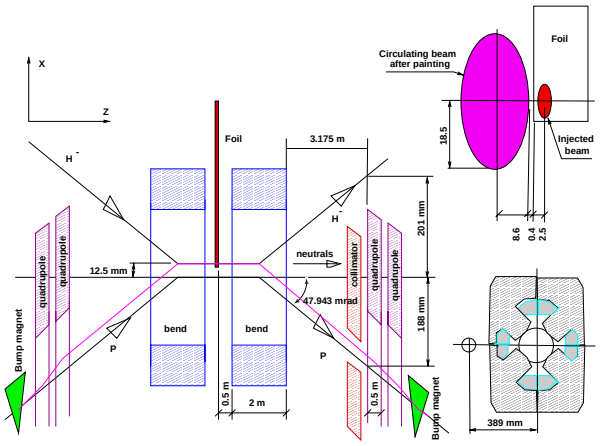

Figure 3: Beam painting scheme.

growth in beam size, show that beam loss rates in the ring without collimation reach 2 kW/m (Fig. 4) which is significantly higher than the above limits.

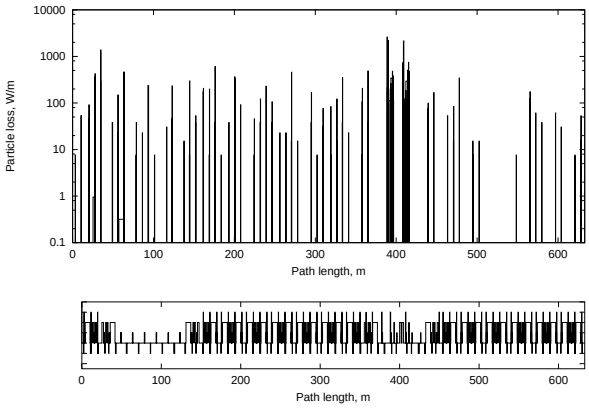

Figure 4: Beam loss in the lattice without collimation.

With that in mind, the purpose of the beam halo cleaning system is to localize proton losses in a specially shielded short section, in this way reducing irradiation of the rest of the machine to the prescribed levels. A beam collimation system has been designed using the available space in the injection straight section and consists of horizontal and vertical primary collimators (scatterers) and five secondary collimators (Fig. 2).

For stable operating conditions, the beam size grows slowly, resulting in a small step size in the impact parameter of halo protons on the collimators of the order of a few μm. A thin primary collimator, when introduced into the lattice as a limiting aperture, increases this proton amplitude due to multiple Coulomb scattering and thus drastically increases the proton impact parameter on subsequent downstream secondary collimators. The net result is a significant reduction of the out-scattered proton yield and total beam loss in the machine components. In addition, it decreases localized overheating of collimator jaws and miti-

gates stringent requirements on the collimator alignment.

Table 2: β-functions at the collimators and phase advance between the primary and secondary collimators.

Collimator	β-function (m)		Phase advance (deg)	
	horizontal	vertical	horizontal	vertical
Primary	23.46	5.11	0	0
COLL-1	24.16	4.76	157	57
COLL-2	15.94	5.82	231	120
COLL-3	20.35	6.99	353	279
COLL-4	17.69	10.46	175	18
COLL-5	13.82	9.48	212	349

Secondary collimators need to be placed at phase advances which are optimal to intercept most of particles out-scattered from the primary collimators during the first turn after the beam halo interacts with the primary collimator. The phase space of the protons at the collimators is shown in Fig. 5. The optimal phase advance is around $k \cdot \pi \pm 30^o$. Phase advances between the primary and secondary collimators are presented in Table 2. All horizontal secondary collimators and vertical COLL-4 and COLL-5 have good phase advances with respect to the primary collimator.

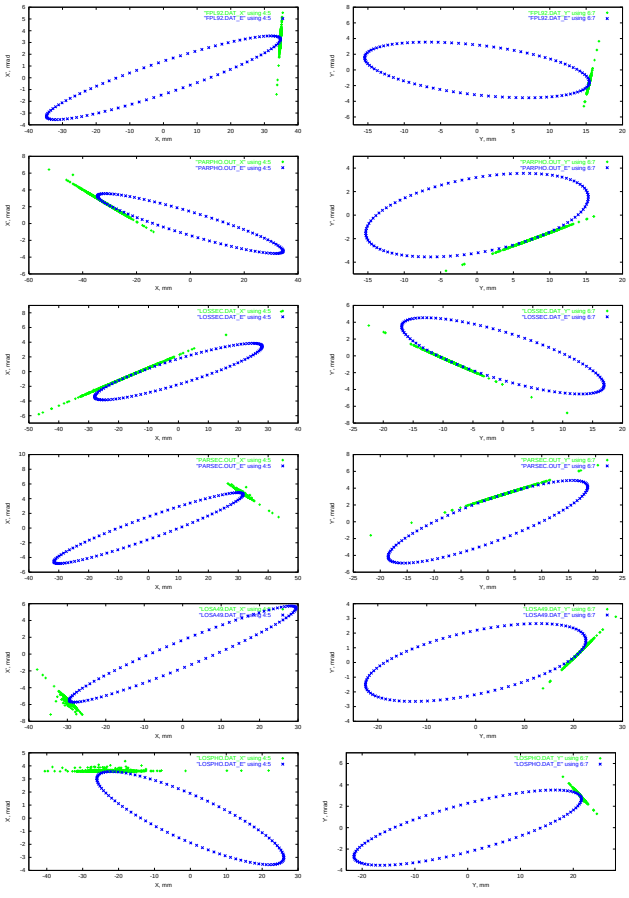

Figure 5: Horizontal (left) and vertical (right) phase space at the primary collimator (top), and at the five secondary collimators.

Calculated beam loss distributions are shown in Fig. 6. Here a primary collimator (1-mm thick tungsten) is positioned at the edge of the beam after painting, while the secondary collimators (0.5-m long steel) are positioned farther from the beam at various distances. Secondary collimators still generate out-scattered particles lost later in the lattice. One can reduce this component with a *3-stage collimation system* positioning several *main* secondary collimators close to the beam to deal with protons scattered in the primary collimator and several *supplementary* collimators farther from the beam to catch particles out-scattered from the main secondary collimators. With a supplementary collimator COLL-4 at 5 mm from the beam, peak losses at S=460 m are down from 20 to 2 W/m. Additional collimator COLL-5 further reduces losses in the ring. Particle loss in the accelerator using different sets of collimators are presented in Table 3.

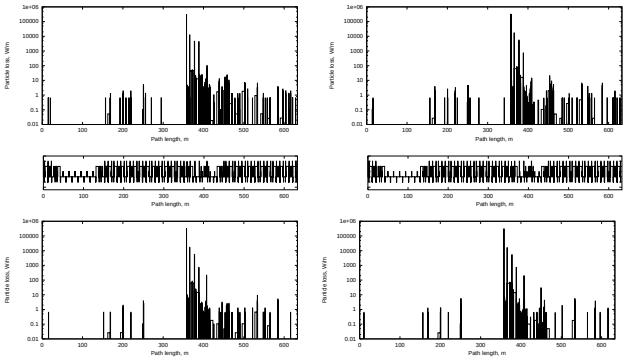

Figure 6: 16-GeV beam loss distributions in the lattice. *Top, left*: COLL-1,2,3 at 0.5 mm. *Top, right*: COLL-1,2 at 0.5 mm, COLL-3 at 3 mm. *Bottom, left*: COLL-1,2 at 0.5 mm, COLL-3 at 3 mm, COLL-4 at 5 mm. *Bottom, right*: The same, with additional COLL-5 at 5 mm.

The thickness and material of primary collimators affect the out-scattered proton angular distribution and nuclear interaction rate. Such a thin scatterer should give a considerable angular kick to the halo particles, but their amplitude should remain smaller than the machine aperture on their way to the secondary collimators. Calculated beam losses are presented in Fig. 7 and in Table 4 for tungsten collimators of several thicknesses with 0.5-m long steel collimators COLL-1 and COLL-2 at 0.5 mm, COLL-3 at 3 mm and COLL-4,5 at 5 mm from the beam edge. A 1 mm collimator provides minimal peak loss rate in the ring.

The β-function varies along the length of a secondary collimator, therefore the collimator apertures are assumed to be tapered follow the beam envelope after the painting. Longer secondary collimators reduce the punchthrough probability and we found that at 16 GeV the minimal length is 0.5 m of steel. As Table 2 and Fig. 8 show, the optimal length is close to 1 m.

According to our calculations 99.82% of beam halo can be intercepted in the collimation section (path length from 358 m to 450 m). The rest is lost outside the collimation section along the machine length of 541 m with average loss

Table 3: Beam loss at 16 GeV: *a)* upstream of the collimation region, *b)* downstream of that, *c)* total in the ring, *d)* peak loss rate in the ring.

Collimator		Beam loss			
Name	Offset	*a*	*b*	*c*	*d*
	mm	%	%	%	W/m
COLL-1	0.5				
COLL-2	0.5	0.072	4.511	4.583	99.9
COLL-3	0.5				
COLL-1	0.5				
COLL-2	0.5	0.099	0.534	0.633	20.2
COLL-3	3.0				
COLL-1	0.5				
COLL-2	0.5				
COLL-3	3.0	0.045	0.233	0.278	5.6
COLL-4	5.0				
COLL-1	0.5				
COLL-2	0.5				
COLL-3	3.0	0.047	0.131	0.177	5.6
COLL-4	5.0				
COLL-5	5.0				

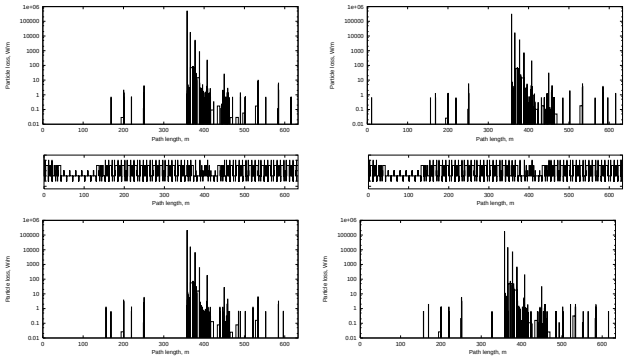

Figure 7: Beam loss with 0.5 mm (top, left), 1 mm (top, right), 2 mm (bottom, left), and 3 mm (bottom, right) thick primary tungsten collimators.

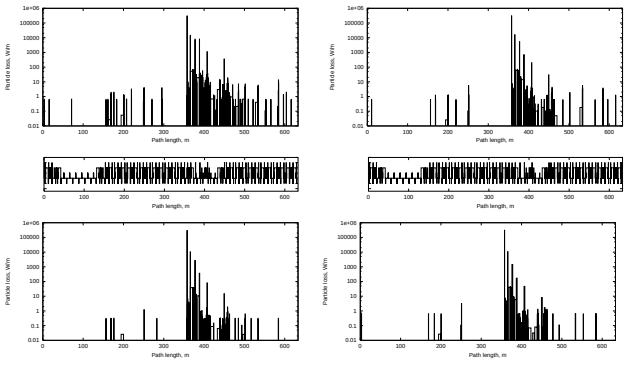

Figure 8: Beam loss distributions for 0.25 and 0.5-m (top) and for 1 and 2 m (bottom) long secondary collimators.

Table 4: Beam loss at 16 GeV *vs* primary collimator thickness *t*: *a)* upstream of the collimation region, *b)* downstream of that, *c)* total in the ring, *d)* peak loss rate in the ring.

	Beam loss			
t	*a*	*b*	*c*	*d*
mm	%	%	%	W/m
0.5	0.038	0.183	0.221	8.7
1.0	0.047	0.131	0.177	5.6
1.5	0.052	0.128	0.180	5.6
2.0	0.054	0.138	0.192	6.2
3.0	0.062	0.114	0.176	9.4

Table 5: Peak loss rate (W/m) in the ring at 16 GeV *vs* secondary collimator length *L*: *a)* upstream of the collimation region, *b)* downstream of that.

L (m)	*a*	*b*
0.25	3.8	18.1
0.50	5.6	5.6
1.00	1.9	1.9
2.00	3.0	1.6

of 0.3 W/m. At several locations, the peak loss rate is up to 5.6 W/m exceeding the tolerable limits. These locations can be locally shielded. Beam loss rates in the collimation system section itself are very high implying a special shielding design. Collimators, magnets and other equipment in the utility section require special cooling as well as fast disconnects and remote control.

3 INJECTION

A practicality in a rapid cycling proton synchrotron dictates a stationary collimator approach with collimator jaws in a fixed position with respect to the beam orbit during the entire cycle. With 10% of intensity lost at injection, 1% at the top energy, and the collimator positions described in the previous section, the calculated beam loss distributions at injection and top energy are shown in Fig. 9. At injection, the peak loss rate in the lattice outside the collimation system is only 0.1 W/m compared to 5.6 W/m at 16 GeV.

4 PERFORMANCE IMPROVEMENT

The same 1 mm thick primary collimator is used as a compromise between the energy loss in the collimator at injection and collimation efficiency at top energy. At injection, halo protons loose a significant fraction of their momentum in such a collimator, resulting in increased beam loss downstream as compared to halo protons at the top energy. To decrease these losses, three additional collimators can be installed in the system in horizontal and vertical planes at 3 mm from the beam edge. Corresponding beam loss dis-

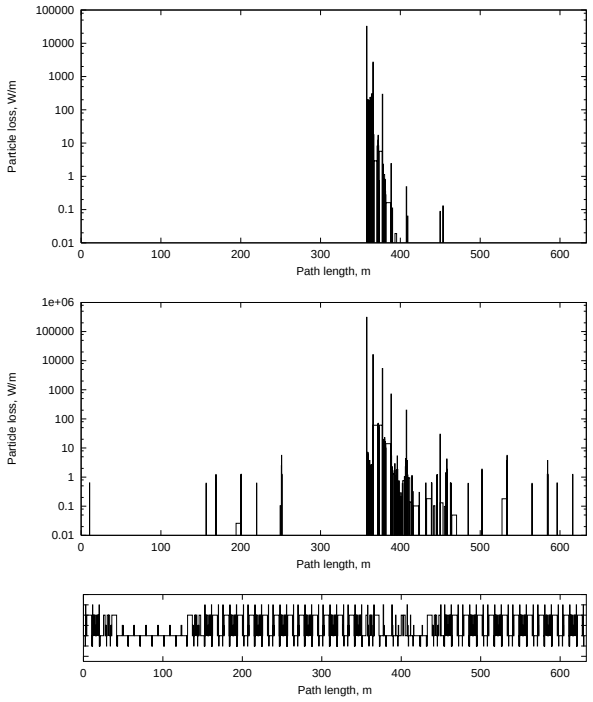

Figure 9: Beam loss at injection (top), and at the top energy (bottom).

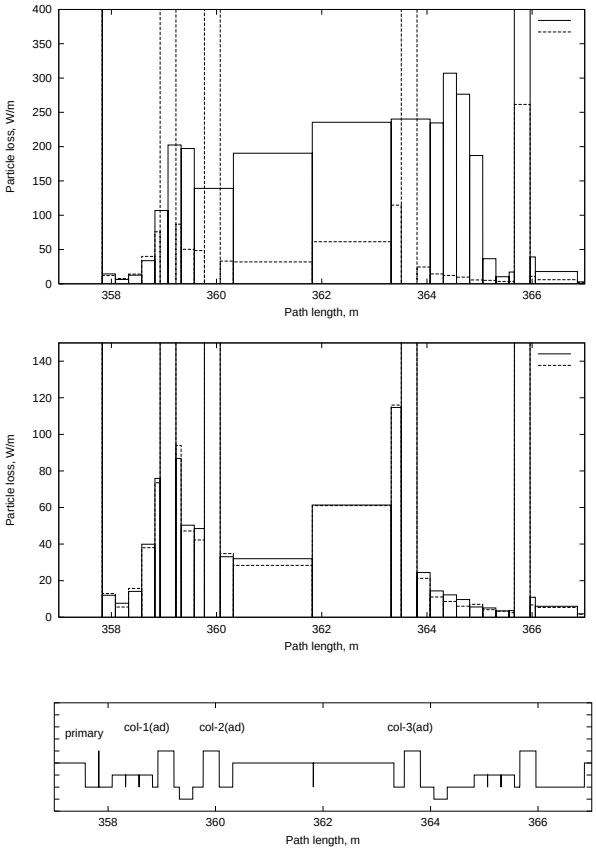

Figure 10: Beam loss at injection immediately downstream of the primary collimator. *Top*: baseline (solid) and with additional collimators (dashed). *Bottom*: with additional collimators non-magnetized (solid) and magnetized (dashed).

tributions in the collimation section are shown in Figs. 10 and 11. These additional collimators increase slightly particle loss in the first 10 m of the collimation system at the top energy (from 5 W/m to 8 W/m), but reduce losses at injection in that region by a factor of four (from 240 W/m to 60 W/m). As shown in Fig. 12, beam loss in the rest of the machine doesn't change with the additional collimators.

Magnetization of these additional collimators to 0.4 T reduces losses by 10% as shown at the bottom of Figs. 10 and 11. The r.m.s multiple Coulomb scattering angle in the steel collimator of one radiation length (17.6 mm) is equal to 16 mrad at injection. Deflection by the 0.4 T magnetic field at the same length is 2.2 mrad only; therefore magnetization does not improve collimator performance noticeably.

5 CONCLUSIONS

A proposed beam collimation system allows more than 99% of the beam loss to be localized in a specially designed region of the injection section. The system consists of a 1-mm thick tungsten primary collimator sitting at the edge of the beam after painting, and two main secondary collimators which are positioned with 0.5-mm offset with respect to the primary collimators. Supplementary secondary collimators placed with 3 mm and 5 mm offset are used to catch the protons emitted from the main secondary collimators. All secondary collimators are 0.5-m long copper with the aperture tapered according to the beam envelope after painting. At 16 GeV beam loss rates outside the collimation section are on average 0.3 W/m which is below the tolerable limits. The peak loss rates at several locations reach 5.6 W/m, and will require local shielding. At injection maximum beam loss rates in the arcs are below 0.1-0.3 W/m.

6 REFERENCES

[1] S. Holmes, editor, "A Development Plan for the Fermilab Proton Source", Fermilab-TM-2021 (1997).

[2] W. Chou, "Proton Driver", these proceedings.

[3] O. E. Krivosheev and N. V. Mokhov, "Tolerable Beam Losses and Shielding", these proceedings.

[4] I. S. Baishev, A. I. Drozhdin and N. V. Mokhov, "STRUCT Program User's Reference Manual", SSCL–MAN–0034 (1994); http://www-ap.fnal.gov/∼drozhdin/STRUCT/STR2.html.

[5] N. V. Mokhov, "The MARS Code System User Guide, Version 13(95)", Fermilab-FN-628 (1995); N. V. Mokhov et al., Fermilab-Conf-98/379 (1998); LANL Report LA-UR-98-5716 (1998); *nucl-th/9812038 v2 16 Dec 1998*; http://www-ap.fnal.gov/MARS/.

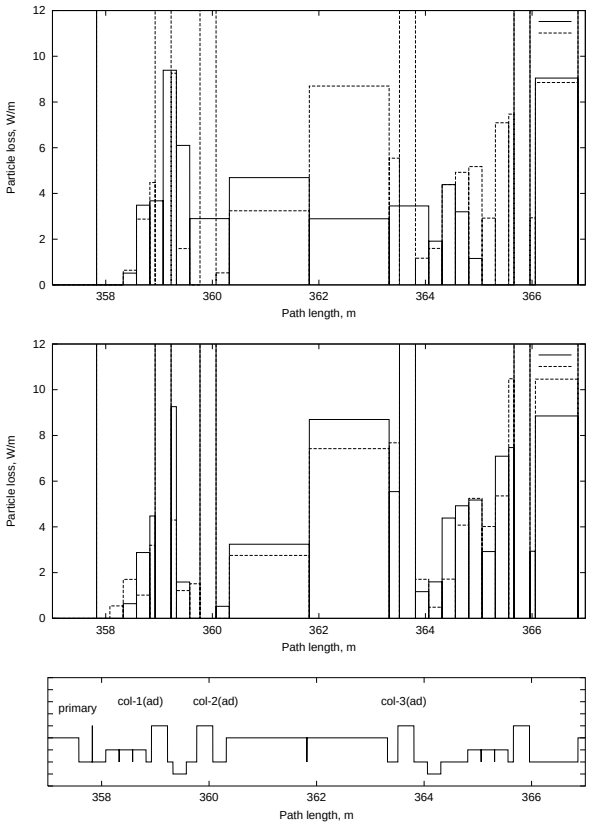

Figure 11: Same as in Fig. 10, at the top energy.

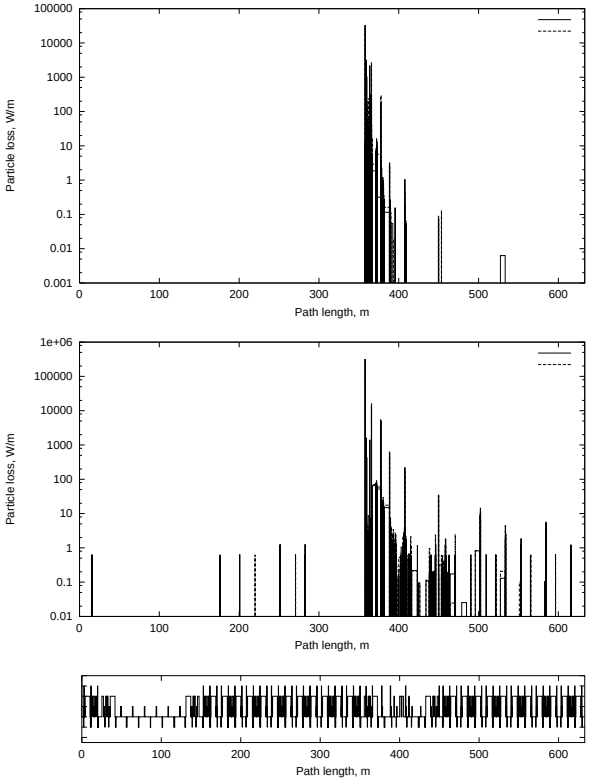

Figure 12: Beam loss in the entire machine at injection (top) and at the top energy (bottom) for the system with (solid line) and without (dashed line) additional collimators.